DEFACTO - battery DEsign and manuFACTuring Optimisation through multiphysic modelling

D.3.1

Date: 31/10/2020

This document is the report on DEM contact model development and parameterization led by TUBS. It contains information of the physical background, implementation and usage of models for the simulation of the structure forming processes during battery electrode processing.

This project has received funding from the European Union's Horizon 2020 research and innovation programme under grant agreement No 875247.

Horizon 2020
European Union Funding
for Research & Innovation

This project has received funding from the European Union's Horizon 2020 research and innovation programme under grant agreement No 875247

Project details

Project acronym	DEFACTO	**Start / Duration**	*01/01/2020 (42 months)*
Topic	LC-BAT-6-2019	**Call identifier**	*H2020-LC-BAT-2019-2020*
Type of Action	RIA	**Coordinator**	*CIDETEC*
Contact persons	*Elixabete Ayerbe*		
Website	**www.defacto-project.eu**		

Deliverable details

Number	*3.1*		
Title	*Report on DEM contact model development and parameterization*		
Work Package	*WP3*		
Dissemination level	Public	**Nature**	*Report*
Due date (M)	10	**Submission date (M)**	
Deliverable responsible	**TUBS**	**Contact person**	***Silas Wolf***

Horizon 2020
European Union Funding
for Research & Innovation

This project has received funding from the European Union's Horizon 2020 research and innovation programme under grant agreement No 875247

Deliverable Contributors

	Name	Organisation	Role / Title	*E-mail*
Deliverable leader	Silas Wolf Mark Lippke Carsten Schilde Arno Kwade	TUBS	Battery modelling engineers Project supervisor Project supervisor	s.wolf@tu-bs.de m.lippke@tu-bs.de c.schilde@tu-bs.de a.kwade@tu-bs.de
Contributing Author(s)				
Reviewer(s)	María Yáñez	CID	Project Coordinator	myanez@cidetec.es
	Elixabete Ayerbe	CID	Project Coordinator	eayerbe@cidetec.es
Final review and quality approval	María Yáñez	CID	Project Coordinator	myanez@cidetec.es

Document History

Date	Version	Name	Changes
19/09/2020	V1	Silas Wolf	First version
23/10/2020	V2	María Yáñez, Elixabete Ayerbe	Revision by Coordinator
28/10/2020	V3	Silas Wolf	Minor changes
29/10/2020	V4	María Yáñez,	Final version

Horizon 2020 European Union Funding for Research & Innovation

This project has received funding from the European Union's Horizon 2020 research and innovation programme under grant agreement No 875247

Content

Horizon 2020 European Union Funding for Research & Innovation

This project has received funding from the European Union's Horizon 2020 research and innovation programme under grant agreement No 875247

1 Executive Summary

This report aims at describing the various models developed in Task 3.1 and applied in Tasks 3.2, 3.3 and 3.4 for the simulation of the electrode process chain. It will first give a short overview over the software that is used to apply the respective models and then proceed on presenting the already included models for the numerical analysis of the structure defining electrode processing steps. Afterwards, models that have been or will be implemented into the particular simulation code are explained in more detail, including a brief explanation about parametrization of the models. First validation results for the correct implementation of some models are given.

2 Acronyms and abbreviations

CBM	Carbon black-binder matrix
CFD	Computational Fluid Dynamics
DEM	Discrete Element Method
DLVO	Derjaguin, Landau, Verwey, Overbeek
LAMMPS	Large-scale Atomic/Molecular Massively Parallel Simulator
LIGGGHTS	LAMMPS improved for general granular and granular heat transfer simulations
MC	Multi contact
OpenFOAM	Open Source Field Operation and Manipulation
VOF	Volume of fluid method

Horizon 2020 European Union Funding for Research & Innovation

This project has received funding from the European Union's Horizon 2020 research and innovation programme under grant agreement No 875247

3 Introduction

The structure formation process during the electrode processing is crucial for the later performance of the battery cell. Characteristics of the battery electrodes such as porosity, tortuosity, pore size distribution, particle size distribution and binder distribution strongly influence the electrochemical performance of the battery. The goal of WP3 “Modelling and simulation of electrode processing” is to simulate the structure formation process as function of the formulation of the electrode slurry and the process parameters during mixing, drying and calendering. Therefore, models have to be developed and implemented into the simulation software to describe the underlying processes that lead to the final electrode structure.

4 Software

This section presents the simulation software used in WP3 of the DEFACTO project. The software needed for performing Computational Fluid Dynamics (CFD) is described as well as the discrete element method code (DEM) for performing particle simulations. Finally, an approach for coupling both methods for simulating particle-fluid interactions is introduced.

4.1 OpenFOAM

OpenFOAM (Open Source Field Operation and Manipulation) is a C++ based open source CFD software mainly using the finite volume method for solving the Navier Stokes equations in an iterative manner. It includes tools for generating meshes to spatially discretize the simulation domain as well as post processing tools. The software used in this WP is based on OpenFOAM 4.X, released by the OpenFOAM foundation in 2017.

4.2 LIGGGHTS

LIGGGHTS (LAMMPS improved for general granular and granular heat transfer simulations) was developed at Johannes Kepler University Linz and further distributed by DCS Computing as an extension of the molecular dynamics software LAMMPS (Large-scale Atomic/Molecular Massively Parallel Simulator). It adds capabilities to model the behaviour of granular systems by solving Newton’s second law of motion based on particle contact models. The release used in this project is an academic version based on LIGGGHTS 3.0.0 from 2014.

4.3 CFDEMcoupling

The CFDEMcoupling software serves as a link between OpenFOAM and LIGGGHTS in the framework of OpenFOAM. It was developed at the Johannes Kepler University Linz and enables the calculation of interaction forces between the fluid, calculated by CFD, and the particles, modelled by DEM. It can be used for unresolved CFD-DEM coupling as well as for resolved CFD-DEM coupling based on the immersed boundary method. In this project, CFDEMcoupling based on version number 19.02 is being used.

Horizon 2020
European Union Funding
for Research & Innovation

This project has received funding from the European Union’s Horizon 2020 research and innovation programme under grant agreement No 875247

5 Contact Models already implemented in the Simulation Software

The following section describes the models needed for the purpose of WP3 that are already implemented in the simulation software and, therefore, are not part of model development in this work package. They are presented for the sake of completeness to highlight the need for the implementation of additional models into the Software.

5.1 DEM contact models

5.1.1 Hertz-Mindlin model

Contact models calculate the forces $\boldsymbol{F}$ between particles when they come into contact or are close to each other. The most common contact model in DEM is the so called Hertz model. The Hertz model has an elastic nature, but elasto-plastic behaviour can be achieved by adding a velocity-dependent damping term (See Equation 1). k_n and k_t descripe the stiffness in normal and tangential direction, v_n and v_t represent the relative velocity in normal and tangential direction, γ_n and γ_t express the velocity depending damping in each direction and δ_t and δ_n are the normal and tangential overlap.

$$\boldsymbol{F} = (k_n\,\delta_n - \gamma_n\,\boldsymbol{v_n}) + (k_t\,\delta_t - \gamma_t\,\boldsymbol{v_t}) \tag{1}$$

5.1.2 Thornton-Ning model

While the Hertz model shows sufficient results for the calendering of graphite anodes, for NMC cathodes the Hertz model overestimates the resistance of the electrode against deformation. For cathodes, good agreements between simulations and experiments were achieved using the so-called Thornton-Ning model. This model firstly calculates the elastic contact deformation according to Hertz and considers an elasto-plastic deformation when a certain yield point is reached. In the elasto-plastic zone, the force displacement relationship $\boldsymbol{F_{el-pl}}$ is expressed as:

$$\boldsymbol{F_{el-pl}} = \boldsymbol{F_y} + \pi\,p_y\,R'(\delta - \delta_y) \tag{2}$$

The critical yield pressure p_y can be related to the critical yield Force F_y. R' represents the effective radius and δ_y is the critical yield normal contact displacement. Further details can be taken from [1,2]. The unloading is performed according to Hertz theory.

5.2 CFD-DEM interaction models

5.2.1 Drag force models

In CFDEMcoupling a variety of different models exists to calculate the effect of fluid drag on the particles and vice versa. A description of the models with varying complexity can be found on the documentation website of CFDEMcoupling [3]. For unresolved CFD-DEM coupling, where the particles are much smaller than the CFD cells, the force is calculated based on the particle size, the relative velocity between fluid and particle and the volume fraction of particles in one CFD cell.

Horizon 2020 European Union Funding for Research & Innovation

This project has received funding from the European Union's Horizon 2020 research and innovation programme under grant agreement No 875247

5.2.2 Pressure gradient force

The pressure gradient force represents the influence of pressure variation in the surrounding of the particles by calculating

$$\boldsymbol{F_{\nabla p}} = -\nabla p \, V_{Particle} \tag{3}$$

With pressure p and the volume of the particle V.

5.2.3 Viscous force

The viscous force calculates the force acting on particles due to shearing of a viscous fluid and is calculated by

$$\boldsymbol{F_{\nabla \cdot \tau}} = -(\nabla \cdot \boldsymbol{\tau}) \, V_{Particle} \tag{4}$$

Using the shear stress $\boldsymbol{\tau}$.

5.2.4 Immersed boundary method

For resolved CFD-DEM coupling, meaning that the CFD cells are much smaller than the particles, the fluid flow around each particle is calculated precisely. Therefore, the forces acting on the particles can be calculated directly via the immersed boundary method, where the particles occupy the fluid domain by applying a solid void fraction ε. The respective particle velocity is set each time step for the particle-occupied CFD cells. The force acting on each particle can be calculated by

$$\boldsymbol{F_{Drag}} = \sum_{c,i} (-\nabla p + \nu \, \rho \, \nabla^2 \, u)(c) \cdot V(c) \tag{5}$$

For the cells of the solid domain c of particle i using the fluid kinematic viscosity ν, the fluid density ρ and the flow velocity u.

Horizon 2020
European Union Funding
for Research & Innovation

This project has received funding from the European Union's Horizon 2020 research and innovation programme under grant agreement No 875247

6 Models for WP3 implemented in T3.1

6.1 Models for the simulation of the drying process

6.1.1 Extension of the volume of fluid method for evaporation of fluid

For the representation of a fluid-fluid interface acting on particles due to drying, the volume of fluid method (VOF) is used on CFD side. It enables the solution of two fluid phases with different properties by introducing a volume fraction (α) for each phase. The properties of each CFD cell can be calculated by averaging the properties of each phase with the volume fraction. The motion of the fluid phases can be described by the following transport equation:

$$\frac{\delta \alpha}{\delta t} + \nabla \cdot \boldsymbol{u}\, \alpha = 0 \tag{6}$$

As the drying process continues, the fluid-fluid interface recedes and leads to a transport of particles in direction of the current collector. The receding interface can be expressed by introducing a negative source term $\dot{\alpha}$ on the right hand side of the fluid phase transport equation. It represents the change of the phase fractions in one fluid phase over time when no fluid transport occurs, leading to the following transport equation at the fluid-fluid interface cells ($0 < \alpha < 1$):

$$\frac{\delta \alpha}{\delta t} + \nabla \cdot \boldsymbol{u}\, \alpha = -\dot{\alpha}_{ev} \tag{7}$$

By setting the source term to a fixed value, a constant drying rate can be achieved like it is present in the first period of battery electrode drying. This behaviour is validated in Figure 1 in pure fluid CFD simulation by imposing a drying rate of 0.5 µm³ µm^{-2} µs^{-1} resulting in a linear decrease of the fluid film thickness until a final residual value is reached due to the boundary condition at the bottom of the film.

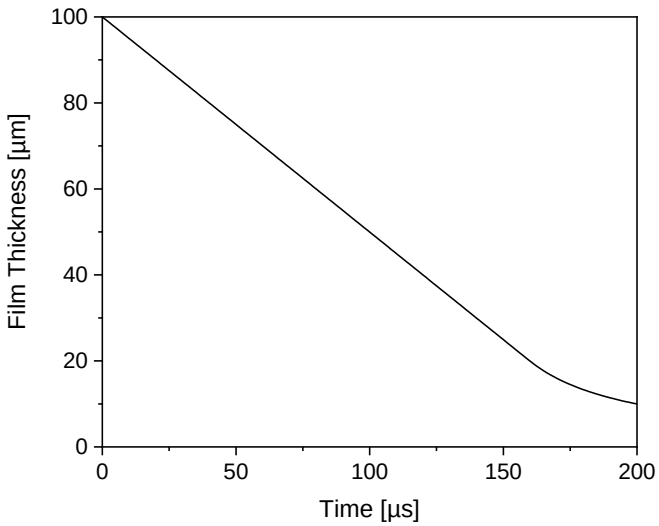

Figure 1: Fluid film thickness over time for an imposed drying rate 0.5 µm³ µm^{-2} µs^{-1} in a CFD simulation

Horizon 2020 European Union Funding for Research & Innovation

This project has received funding from the European Union's Horizon 2020 research and innovation programme under grant agreement No 875247

6.1.2 Capillary force for unresolved CFD-DEM coupling

In order to realize the displacement of the particles by the receding fluid-fluid interface during drying, the action of surface tension acting on the particles needs to be taken into account. For the unresolved CFD-DEM coupling this can be achieved by interpolating the position of the fluid-fluid interface (α = 0.5) to the position of the particle center. Together with the contact angle θ and the surface tension σ as input parameters, the resulting capillary force $\boldsymbol{F_c}$ in vertical direction over the contact line can be calculated according to Breinlinger et al. [4] as:

$$\boldsymbol{F_c} = d_P\, \pi\, \sigma\, \sin(\omega)\ \sin(\omega + \theta)\ \frac{\nabla \alpha_P}{|\nabla \alpha_P|} \tag{8}$$

with ω being the immersion angle and d_P the diameter of the particle. The implementation of the model has been proven to correspond to the analytical solution by placing one particle with its center on the fluid-fluid surface and letting it move to an equilibrium position, with the energy dissipating by the drag force and a high viscosity of 25 mPa·s. The results for the analytical and simulated particle positions at various contact angles are shown in Figure 2.

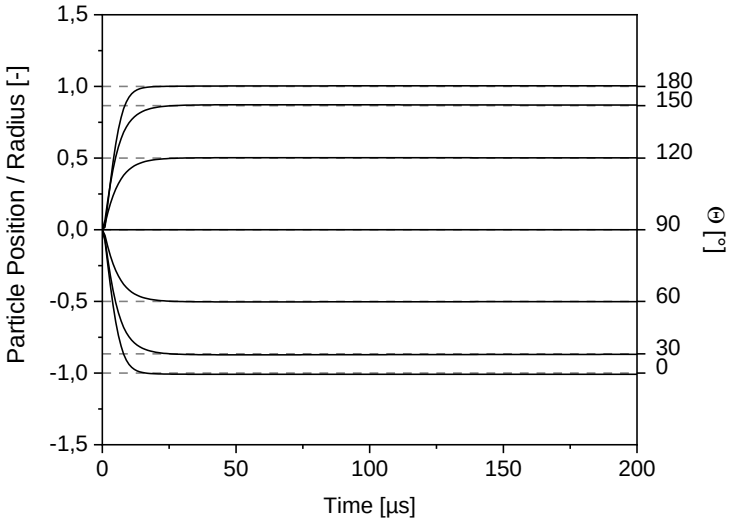

Figure 2: Simulated particle position for various contact angles (solid lines) and their corresponding analytical equilibrium positions over time (segmented lines)

6.1.3 Capillary force for resolved CFD-DEM coupling

When performing resolved CFD-DEM simulations, apart from the fluid drag also the movement of the particles due to capillary forces can be calculated in a much more precise manner with the finer mesh. For this, a contact angle has to be imposed at the three-phase contact line for cells in which a solid-fluid interface as well as a fluid-fluid interface exists. This can be achieved by tuning the surface normal of the fluid-fluid interface n_l accordingly to the contact angle θ following

$$n_l = n_s \cos\theta + t_s \sin\theta \tag{9}$$

with the solid interface normal n_s and the tangent vector at the solid surface t_s [5]. The force acting on the particle can then be divided in two parts: One is the pressure difference according to the Young-Laplace-Equation resulting from the bending of the fluid-fluid interface due to the contact angle. This is already included in the drag force calculation described in Section 5.2.4.

Horizon 2020
European Union Funding
for Research & Innovation

This project has received funding from the European Union's Horizon 2020 research and innovation programme under grant agreement No 875247

The other part is the surface tension acting at the contact line. By solving a volume integral over the particle domain using the following formula, with t_c being the contact line tangent vector and ϕ being the solid volume fraction, the force acting on the particle over the contact line can be calculated [5]:

$$\boldsymbol{F_C = \int_{V_P} \sigma\, t_c(x) \left(\nabla \alpha \cdot t_s(x)\right) \left(\nabla \phi \cdot n_s(x)\right) dV} \quad (10)$$

Using a set up similar to that in Section 6.1.2 but in a resolved manner, the implementation of the contact angle and the capillary force has been investigated. The results, shown in Figure 3, display the formation of a contact angle at the three phase contact line without any forces acting on the particle on the left side. Remarkable is the visible downward bending of the fluid-fluid interface. Calculating interaction forces leads to the movement of the particle in downward direction with the fluid interface following the particle motion. This behaviour has to be further investigated to achieve a non-moving fluid-fluid interface.

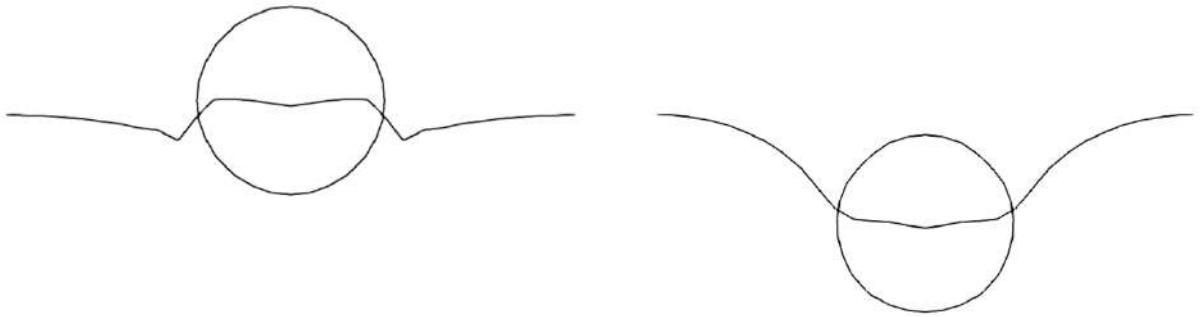

Figure 3: Results of the implementation of a resolved contact angle and the resulting capillary force. A contact angle is enforced at the fluid-fluid-particle boundary by the CFD simulation (left). The acting surface tension pulls the particle downwards, when activating the force calculation (right)

6.1.4 Brownian motion

Small particles suspended in fluids experience a random movement caused by the undirected, temperature driven motion of the surrounding fluid molecules. This leads to diffusion phenomena that have been proven to induce demixing of particles of different sizes during drying processes [6]. The model recently included in our DEM code is based on an approach by Breinliger et al. [7] and calculates new particle positions in random directions by calculating a force F_B with its magnitude and direction derived from the mean squared distance $\bar{x}^2$ that each particle with radius R_P travels during one timestep t:

$$\frac{\bar{x}^2}{t} = \frac{k_B\, T}{2\,\pi\,\eta\, R_P} \quad (11)$$

The movement is dependent on the temperature T and the dynamic viscosity η that have to be set as input parameters for the model.

Horizon 2020 European Union Funding for Research & Innovation

This project has received funding from the European Union's Horizon 2020 research and innovation programme under grant agreement No 875247

6.1.5 Lubrication force

When two particles in suspension approach each other, the fluid in between the two bodies gets displaced in tangential direction. This leads to a pressure gradient in the gap between the particles and to a velocity profile with viscous stresses that induce a hydrodynamic force. This force is called lubrication force and is calculated implicitly in resolved CFD-DEM simulations. For unresolved CFD-DEM coupling, however, a model needs to be included that accounts for this microscopic, potentially structure influencing force. This force has been implemented in the CFD-DEM environment for calculating the forces and torques in normal direction (n) respectively for torsion (t) as well as for sliding particles (s) [8]:

$$\boldsymbol{F_{nl}} = -6\,\pi\,\eta\,R_P\,\boldsymbol{v_r}\cdot\boldsymbol{n}\left(\frac{1}{4}\,\epsilon^{-1} - \frac{9}{40}\log(\epsilon) - \frac{3}{112}\,\epsilon\log(\epsilon)\right) \tag{12}$$

$$\boldsymbol{F_{sl}} = -6\,\pi\,\eta\,R_P\left[\boldsymbol{v_s}\left(-\frac{1}{6}\log(\epsilon)\right) + \boldsymbol{v_{cs}}\left(-\frac{1}{6}\log(\epsilon) - \frac{1}{12}\,\epsilon\log(\epsilon)\right)\right] \tag{13}$$

$$\boldsymbol{M_{sl}} = -8\,\pi\,\eta\,R_p^2\left[(n\times v_s)\left(-\frac{1}{6}\log(\epsilon) - \frac{1}{12}\,\epsilon\log(\epsilon)\right) + (n\times v_{cs})\left(-\frac{1}{5}\log(\epsilon) - \frac{47}{250}\,\epsilon\log(\epsilon)\right)\right] \tag{14}$$

$$\boldsymbol{M_{tl}} = -8\,\pi\,\eta\,R_p^2\left[\left(\Omega_i - \Omega_j\right)\cdot n\right]n\left(\frac{1}{8}\,\epsilon\log(\epsilon)\right) \tag{15}$$

It depends on the relative velocity v_r, the sliding velocity v_s or the angular velocity Ω of the approaching particles as well as their relative distance $\epsilon = d/R_P$ and the fluid viscosity η.

6.1.6 DLVO forces

In order to take into account repulsion and attraction of particles due to electrostatic and van der Waals forces, a force model combining those two effects according to the DLVO theory has been implemented into LIGGGHTS recently. Given the Hamaker constant *A*, the retarding function *f(h)*, the distance of the particle surfaces h, the inverse Debeye length κ, and the interaction constant *Z*, the resulting long range particle-particle interaction force can be calculated as:

$$\boldsymbol{F_{dlvo}} = \boldsymbol{F_{vdw}} + \boldsymbol{F_{ed}} = \frac{r}{2}\left(-A\,f(h)\frac{1}{6\,h^2} + \kappa\,Z\,e^{-\kappa h}\right) \tag{16}$$

With

$$Z = 64\,\pi\,\epsilon_0\,\epsilon\left(\frac{k_B\,T}{e_0}\right)^2\tanh^2\left(\frac{\epsilon_0}{4\,k_B\,T}\,\nu\,\zeta\right) \tag{17}$$

using the permittivity of vacuum ϵ_0, the permittivity ϵ, the Boltzmann constant k_B, the Temperature *T*, the elementary charge e_o, the valence of the ions *v* and the zeta potential ζ.

For parametrizing this model, the input parameters to evaluate are zeta potential, valence, ionic strength, temperature, permittivity and the Hamaker constant.

Horizon 2020 European Union Funding for Research & Innovation

This project has received funding from the European Union's Horizon 2020 research and innovation programme under grant agreement No 875247

6.2 Models for the simulation of the calendering process

6.2.1 Multi contact model

In classical discrete element method, the so-called soft particle approach, particle deformations are mimicked by overlaps between contacting particles. When an overlap is detected, the contact forces between two particles are calculated by a contact law. The general assumption made is that contacts between particles are independent and therefore, contact forces are resolved locally. This assumption is only true in cases when particles deformation is small. When large deformations are occurring, the assumption of contact dependency seized to be valid. One way to tackle this issue is by taking into account the mutual influence of contacts acting simultaneously on a single particle. This need has led to the formulation of a new field, referred as the multi-contact discrete element method (MC-DEM).

More precisely, with the novel multi-contact stress model (MC-stress), the deformation in contrast to classical DEM is now calculated by including the momentary stress state experienced by the particle [8]:

$$\boldsymbol{F_{MC}} = k\,\delta^{a} + \beta\,\nu\,A\,(\sigma_{xx} + \sigma_{yy} + \sigma_{zz}) \tag{18}$$

Here, δ represents the overlap, k is the stiffness factor, a is 1 or 2/3 dependent on which model is used, ν is the Poissons's ratio, β an empirical prefactor and A represents the contact area.

6.2.2 Bond model

The carbon black-binder matrix (CBM) is modelled by solid bonds between particles. In order to mimic the elastic-plastic behaviour of the CBM, bonds are considered as spring-dashpot elements which are created between particles if the distance between them is sufficiently low in relation to their radius. This minimum distance is also used to control the amount of bonds in order to adjust the correct formulation of the virtual electrode. Bonds are able to transfer forces and torques in normal and tangential direction. The bonds have a certain stiffness and ultimate strength, which can be seen more as a calibration parameter than a material constant, since there are multiple assumptions that have been made for the bonds, i.e. their uniform shape and a homogeneous bond composition.

The incremental bond force dF_b, which is added every time step, can be calculated according to equation 19. A represents the cross sectional area of the bond, S corresponds to the stiffness of the bond in respective direction (normal or tangential), and the product of $dt * v$ is the incremental displacement of the bond. The viscous damping is considered by Equation 20. F_b' is the accumulated force before the latest time step and α can be understood as a damping coefficient.

$$d\boldsymbol{F_b} = -v\,S\,A\,dt \tag{19}$$

$$\boldsymbol{F_b} = \alpha\,F_b' + dF_b \tag{20}$$

Gradients in binder concentration within the electrode can be considered by shrinking the radius of bonds in areas of low binder concentration [10].

Horizon 2020 European Union Funding for Research & Innovation

This project has received funding from the European Union's Horizon 2020 research and innovation programme under grant agreement No 875247

6.2.3 Heat transfer through binder bonds

Within the simulation heat transport within the particles and over the particles contacts are differentiated. Furthermore, the heat conduction in the CBM must be taken into account. Therefore, in order to display the use of heated calendaring rolls correctly, a model to transfer heat via bonds has been implemented. Before that, heat could only have been transferred at a direct particle contact. In order to transfer heat via bonds, a specific bond density, specific bond heat capacity and a specific bond-particle thermal contact resistance has to be set. A uniform temperature within the bond is assumed and in each time step, heat is transferred between the bond particles and the bond.

Three different scenarios have to be distinguished: A) Heat transport via direct particle contact, B) Heat transport via a bond connection and C) A hybrid case (See **¡Error! No se encuentra el origen de la referencia.**).

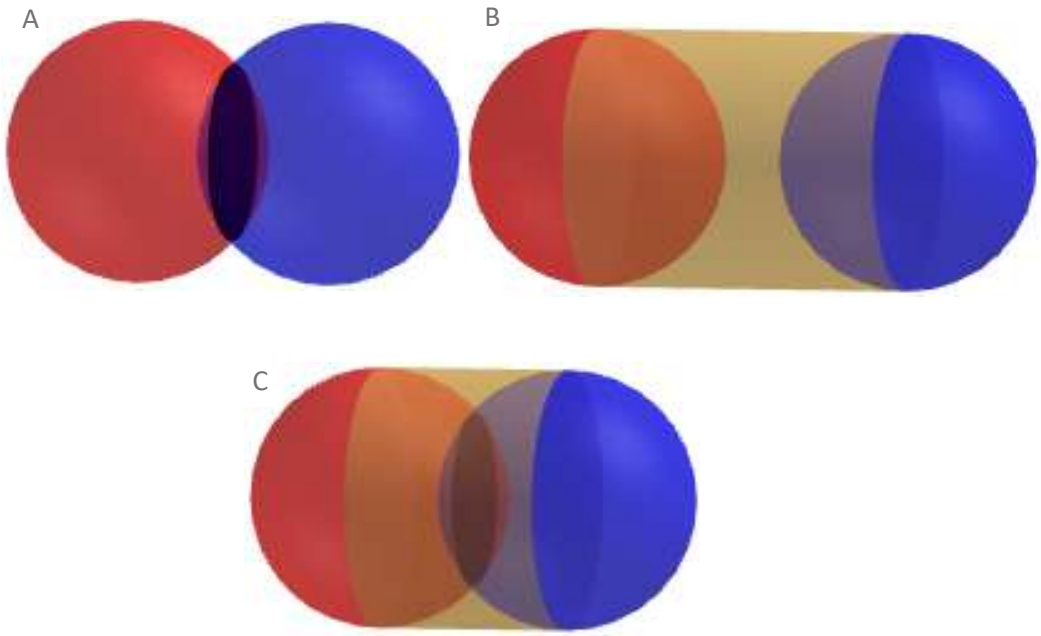

Figure 4: Three different possibilities for heat transfer between particles. A: Direct particle contact. B: Particles connected via bond. C: Particle contact and bond connection.

The heat transfer between the particles *i* and *j* via direct particle contact (**¡Error! No se encuentra el origen de la referencia.**, A) is already implemented in LIGGGHTS:

$$\dot{Q}_{ij} = h_{c;ij}\, dT \tag{21}$$

$$h_{c:ij} = \frac{4\, k_i\, k_j}{k_i + k_j} A_{i,j}^{1/2} \tag{22}$$

The heat transfer rate $Q_{i,j}$ equals the product of the heat transfer coefficient $h_{c;ij}$ and the temperature difference between the particles *i* and *j*. The heat transfer coeffient $h_{c;ij}$ is based on the contact area A_C of both particles in touch and their respective heat conductivity *k* [11, 12].

If the heat is transferred via bonds (**¡Error! No se encuentra el origen de la referencia.**, B), a two-step calculation is used. In the first step, heat is transferred from the warmer particle *i* to the bond and in the second step heat is transferred from the bond to the colder particle *j*. The heat transfer is based on the contact area *A* between the bond and the particles, the temperature of the particles, the

Horizon 2020 European Union Funding for Research & Innovation

This project has received funding from the European Union's Horizon 2020 research and innovation programme under grant agreement No 875247

bond and the heat transfer coefficient h_b. Since h_b is nearly impossible to measure and takes different assumptions, like a uniform bond shape and a homogeneous bond composition into account, it should be seen more as a calibration factor than a physical parameter.

$$\dot{Q}_{iB} = h_{iB}\, A\, (T_i - T_B) \tag{23}$$

$$\dot{Q}_{BJ} = h_{Bj}\, A\, (T_B - T_J) \tag{24}$$

If two particles are in direct contact and also are bonded (See **¡Error! No se encuentra el origen de la referencia.**, C), the contact area of the direct physical contact is deducted from the contact area of the particles and the bond and both calculations are used.

Since contact resistances are very difficult to measure and because of the already discussed model assumptions, the thermal contact resistance should be treated as a calibration factor. However, depending on the temperature the bond stiffness has to be adjusted during the calendering process. In order to develop a function to calculate the bond stiffness for different temperatures, the bond stiffness will be calibrated with preheated electrodes at different temperatures.

7 Conclusions

This report provides an overview over different models that have been implemented in the CFD, DEM and CFD-DEM simulation codes to enable the simulation of the different process steps in electrode production. It shows the most important equations of the models and describes the parameters needed to calculate particle-particle interactions and interconnected interaction forces between particles and fluids. Before applying the models to real life problems, sensitivity studies have to be performed in specified simulation environments to evaluate contact and material models feasibility and impact on the simulation results. Also, calibration of input parameters has to be performed to get meaningful results when applying the models. Nevertheless, the implementation of the presented models builds the foundation of the upcoming work in WP3.

Horizon 2020
European Union Funding
for Research & Innovation

This project has received funding from the European Union's Horizon 2020 research and innovation programme under grant agreement No 875247

8 Literature

[1] Sangrós Giménez, C.; Finke, B.; Schilde, C.; Froböse, L.; Kwade, A.: Numerical simulation of the behavior of lithium-ion battery electrodes during the calendaring process via the discrete element method, Powder Technology 391, 2009, p. 1-11

[2] Thornotn, C.; Ning, Z.: A theoretical model for the stick/bounce behaviour of adhesive, elastic-plastic spheres, Powder Technology 99 (2), 1996, p. 154-162

[3] DCS Computing, CFDEMcoupling documentation, 2016, https://www.cfdem.com/media/CFDEM/docu/CFDEMcoupling_Manual.html#models-solvers, accessed 06/10/2020

[4] Breinlinger, T.; Hashibon, A.; Kraft, T.: Simulation of the influence of surface tension on granule morphology during spray drying using a simple capillary force model, Powder Technology 283, 2015, p. 1-8

[5] Washino, K.; Tan, H. S.; Hounslow, M. J.; Salman, A. D.: A new capillary force model implemented in microscale CFD-DEM coupling for wet granulation, Chemical Engineering Science, 93, 2013, p. 197-205

[6] Zellmer, S.; Garnweitner, G.; Breinlinger, T.; Kraft, T.; Schilde, C.: Hierarchical Structure Formation of Nanoparticulate Spray-Dried Composite Aggregates, ACS nano, 9 (11), 2015, p. 10749–10757

[7] Breinlinger, T.; Kraft, T.: A simple method for simulating the coffee stain effect, Powder Technology, 256, 2014, p. 279-284

[8] Kroupa, M.; Vonka, M.; Soos, M.; Kosek, J.: Utilizing the Discrete Element Method for the Modeling of Viscosity in Concentrated Suspensions, Langmuir, 32, 2016, p. 8451-8460

[9] Bajigirani, K. T.: Elasticity and Wave Propagation in Granular Materials, Dissertation, 2019

[10] Sangrós Giménez, C.; Finke, B.; Nowak, C.; Schilde, C.; Kwade, A.: Structural and mechanical characterization of lithium-ion battery electrodes via DEM simulations, Avanced Powder Technology, 29 (10), 2018, p. 2312–2321

[11] DCS Computing, LIGGGHTS documentation, 2016, https://www.cfdem.com/media/DEM/docu/Manual.html, accessed 17/09/2020

[12] Chaudhuri, B.; Muzzio, F. J.; Tomassone, M. S.: Modeling of Heat Transfer in Granular Flow in Rotating Vessels, Chemical Engineering Science, 61 (19), 2006, p. 6348-6360

Horizon 2020 European Union Funding for Research & Innovation

This project has received funding from the European Union's Horizon 2020 research and innovation programme under grant agreement No 875247